PHYSICAL REVIEW B **83**, 041202(R) (2011)

Candidates for topological insulators: Pb-based chalcogenide series

Hosub Jin,[1] Jung-Hwan Song,[1,*] Arthur J. Freeman,[1] and Mercouri G. Kanatzidis[2]
[1]*Department of Physics and Astronomy, Northwestern University, Evanston, Illinois 60208, USA*
[2]*Department of Chemistry, Northwestern University, Evanston, Illinois 60208, USA*

(Received 21 December 2010; published 31 January 2011)

We theoretically predict that the series of Pb-based layered chalcogenides, $Pb_nBi_2Se_{n+3}$and $Pb_nSb_2Te_{n+3}$, are possible new candidates for topological insulators, and the topological phases are changed from a topological insulator to a band insulator with increasing n. Among the new topological insulators, we found a large bulk band gap of 0.40 eV in $PbBi_2Se_4$, and that of $Pb_2Sb_2Te_5$ is located near the phase boundary between a trivial and a nontrivial topological insulator, which raises the possibility of tuning the topological phase by changing the external parameters.

DOI: 10.1103/PhysRevB.83.041202 PACS number(s): 71.20.Nr

Topological insulators, distinguished from normal band insulators by a nontrivial Z_2 topological number and topologically protected surface states, have attracted a great deal of attention due to their significance both for applications and for fundamental research on a new quantum state of matter.[1–3] Since the suggestion of a quantum spin Hall effect in a honeycomb lattice,[4,5] which is a time-reversal pair of Haldane models[6] induced by spin-orbit interactions, several topological insulator materials were predicted and observed.[7–13] To date, Bi_2Se_3 is known as the best three-dimensional (3D) high-temperature topological insulator with a large bulk band gap, one simple surface-state Dirac cone, and a simple surface geometry from the layered crystal structure and van der Waals–type interlayer interactions. Efforts to find new topological insulators are still being made.[14,15] A large spin-orbit coupling (SOC) strength is essential to realizing nontrivial topological band structures.

To classify the Z_2 topological number, we adopted the method proposed in Ref. 16, which studied the topological phase transition by making a variation of external parameters such as the SOC strength or lattice constants. In our work, we varied the SOC strength (λ_{SO}) from 0 to the real values of the systems (λ_0), and investigated whether the topological phase transition occurs. In 3D topological insulator materials, a band crossing between conduction and valence bands should occur during this process: the 3D Dirac cone appears only at the transition point between the band insulator (BI) and topological insulator (TI).

There are several advantages to this method. First, it is intuitive and only needs a direct observation of the Dirac cone at the transition point. Second, it does not require a heavy computational cost because of the simple unit-cell calculations. The surface calculations to see the topologically protected surface state are also one of the alternative ways to determine the topological phase. The degrees of complexity of such calculations are, however, greater than the method we employed here. Third, this method can be applied to every system regardless of the existence of inversion symmetry. Lastly, the critical SOC value at which the band crossing occurs shows how far the system is located from the phase boundary of BI and TI.

By using this method, we found that the series of Pb-based chalcogenides, $Pb_nBi_2Se_{n+3}$ and $Pb_nSb_2Te_{n+3}$, are possible new candidates for TI materials. As n increases, the phase transition from TI to BI is found to occur between $n = 2$ and 3 for both series. Significantly, among the new TI's, we found a bulk band gap of 0.40 eV in $PbBi_2Se_4$, which is one of the largest gap topological insulators, and we found that $Pb_2Sb_2Te_5$ is located in the immediate vicinity of the topological phase boundary, making its topological phase easily tunable by changing external parameters such as lattice constants. Due to the 3D Dirac cone at the phase boundary, massless Dirac fermions also may be easily accessible in $Pb_2Sb_2Te_5$.

To investigate the electronic structures and topological phases, first-principles calculations were performed using the full-potential linearized augmented plane wave method[17] with the gradient-corrected Perdew, Burke, and Ernzerhof form of the exchange-correlation functional.[18] The core states and the valence states were treated fully relativistically and scalar relativistically, respectively. The SOC was included by a second variational procedure.[19,20] The calculations were carried out with the experimental lattice parameters for bulk $PbBi_2Se_4$, $PbSb_2Te_4$, and $Pb_2Bi_2Se_5$, and with the fully optimized geometry for the others, because crystal structures of $n = 1$ compounds and $Pb_2Bi_2Se_5$ were reported experimentally[21–23] and those of other n's are designed here theoretically. The muffin-tin radii of Pb, Bi, and Se are 3.0, 2.9, and 2.4, respectively.

$PbBi_2Se_4$ and $PbSb_2Te_4$ have a rhombohedral crystal structure and a layered structure stacked along the c axis of the hexagonal lattice, consisting of seven atoms in one septuple layer. The Pb atom is sandwiched by Se-Bi-Se or Te-Sb-Te layers and located at the inversion center, shown in Fig. 1(a). There are van der Waals interactions between two septuple layers, and this provides a natural surface geometry that is appropriate for observing a topologically protected surface state.

Upon increasing the SOC strength ratio, λ_{SO}/λ_0, from 0 to 1, both materials show the phase transition from BI to TI; in other words, there are band crossings during the process, cf., Figs. 1(b)– 1(d) and Figs. 1(f)–1(h). Critical values of the ratio are 0.46 for $PbBi_2Se_4$ and 0.62 for $PbSb_2Te_4$, and the electronic band structures at each critical point are shown in Figs. 1(c) and 1(g). 3D Dirac cones are seen at the Z point, one of the time-reversal invariant momentum points where $-\mathbf{k}$ is equivalent to $\mathbf{k}$; they are doubly degenerate due to spatial inversion and time-reversal symmetry.

Without the spin-orbit interaction, the system should have a trivial Z_2 topological number ($\nu = 0$), the so-called BI. The presence of band crossings between conduction and valence

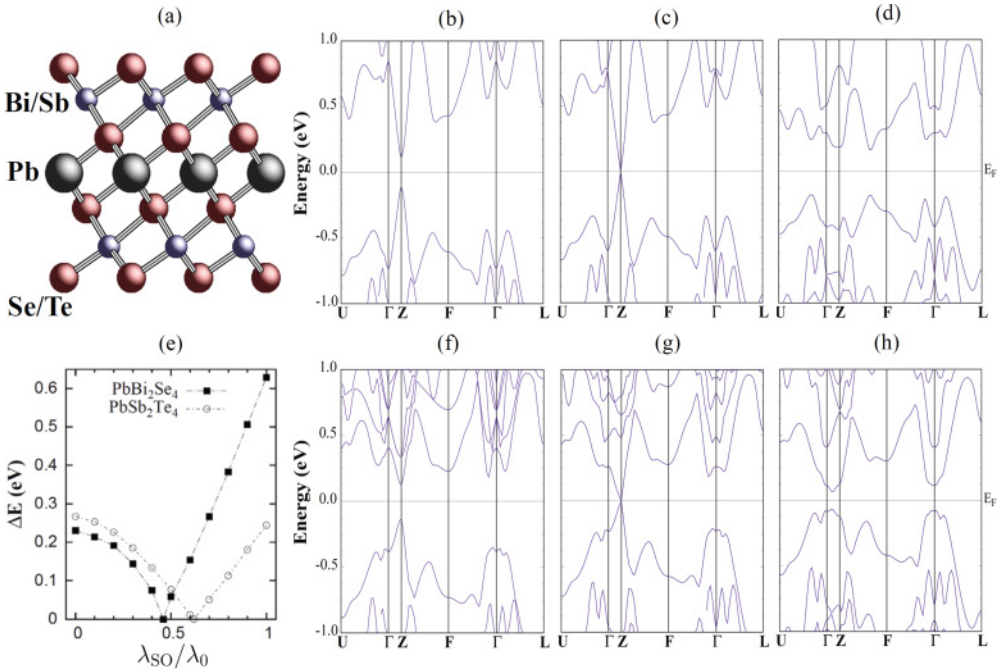

FIG. 1. (Color online) (a) Crystal structures of $PbBi_2Se_4/PbSb_2Te_4$, electronic band structures of (b)–(d) $PbBi_2Se_4$ and (f)–(h) $PbSb_2Te_4$, and (e) energy difference between conduction and valence bands at the Z point. Calculations (b),(f) without spin-orbit interactions ($\lambda_{SO} = 0$); (d),(h) with real SOC strength ($\lambda_{SO} = \lambda_0$); and (c),(g) with critical SOC strength ($\lambda_{SO} = \lambda^c_{SO}$).

bands during increasing SOC represents the change of its Z_2 topological number from trivial ($\nu = 0$) to nontrivial ($\nu = 1$) insulators. If the topological phase transition occurs before the SOC strength reaches λ_0, the system is classified as TI. In these inversion-symmetric systems, band crossing is equivalent to band inversion where conduction and valence bands exchange their parities at the crossing point.

From our calculations, the bulk gaps of $PbBi_2Se_4$ and $PbSb_2Te_4$ are indirect and 0.28 and 0.13 eV, respectively. The gap size of $PbBi_2Se_4$ is comparable to that of Bi_2Se_3.[12,13] The gap values from the calculations without SOC are the direct band gap of 0.23 eV [Fig. 1(b)] and 0.27 eV [Fig. 1(f)] at the Z point, which reflects purely hybridization effects. In Fig. 1(e), the energy difference between the conduction and valence bands (ΔE) at the Z point, where the band inversion occurs, is plotted as a function of the SOC strength. After increasing the SOC strength, ΔE shrinks to zero and then increases again, which shows the competition between hybridization and SOC strength in the topological phase transition. The larger slope of $PbBi_2Se_4$ at the phase-transition point indicates the stronger SOC strength compared to $PbSb_2Te_4$. A nontrivial topological phase is a result of the predominance of SOC over the hybridization strength. Compared to other TI chalcogenides, the large band gap in $PbBi_2Se_4$ originates from weak hybridization and large SOC strength.

To estimate the gap size of $PbBi_2Se_4$ more precisely, we performed nonlocal screened-exchange local-density-approximation (sX-LDA) calculations,[24,25] which overcome the well-known weakness of gap underestimation in the LDA scheme and reproduce the experimental gap values in many semiconducting materials. Significantly, the sX-LDA result yields a gap of 0.40 eV in $PbBi_2Se_4$, which confirms that $PbBi_2Se_4$ is one of the largest gap TI's, leading to the fact that $PbBi_2Se_4$ may be the best for high-temperature applications among the known TI materials.

One advantage of the method used in this work to verify the topological phase is that it describes the exact distance from the phase boundary of BI and TI in terms of the SOC strength. For instance, the larger critical SOC strength of $PbSb_2Te_4$ than that of $PbBi_2Se_4$ means that the former is closer to the phase boundary than the latter.

In addition to $PbBi_2Se_4$ and $PbSb_2Te_4$, we suggest the series of $Pb_nBi_2Se_{n+3}$ and $Pb_nSb_2Te_{n+3}$ structures, where n is an integer larger than 1, and we show that a phase transition from TI to BI occurs as n increases. The crystal structure of $Pb_nBi_2Se_{n+3}/Pb_nSb_2Te_{n+3}$ is composed of a $(PbSe)_n/(PbTe)_n$ core with Se-Bi-(Se)/Te-Sb-(Te) sandwich layers. As shown in Fig. 2(a), the critical SOC ratio (λ^c_{SO}/λ_0)

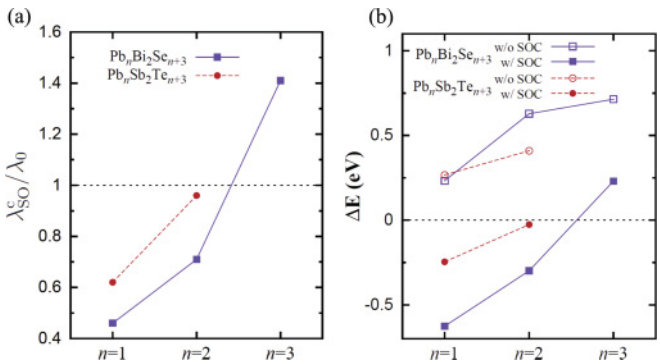

FIG. 2. (Color online) With respect to n for the $Pb_nBi_2Se_{n+3}$ and $Pb_nSb_2Te_{n+3}$ series, (a) critical SOC ratio and (b) energy difference between conduction and valence bands with or without SOC at the point where the band inversion occurs. ΔE is always positive and the negative sign in (b) only indicates the nontrivial topological phase.

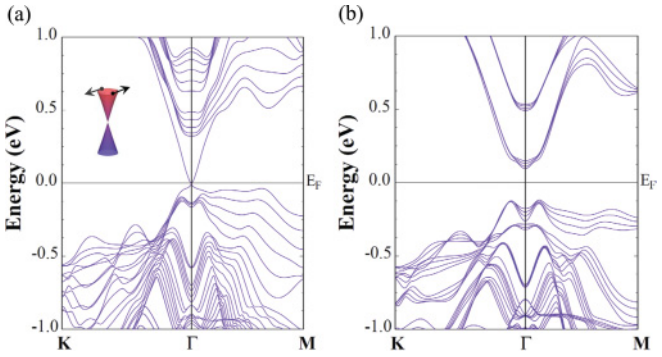

FIG. 3. (Color online) Band structures of slab geometry of (a) six septuple layers of $PbBi_2Se_4$ and (b) four hendecuple layers of $Pb_3Bi_2Se_6$, which represent TI and BI, respectively.

exceeds 1 for $n \geqslant 3$ for both series of materials, which means that there is a phase boundary between $n = 2$ (TI) and $n = 3$ (BI). Figure 2(b) shows the energy difference between the conduction and valence bands at a certain point in the Brillouin zone[26] where the 3D Dirac cone appears at the topological phase-transition point. The negative sign of ΔE indicates a nontrivial topological phase, whereas it is positive for the trivial BI phase. From the calculations without SOC, ΔE has a tendency to rise monotonically with n, which means that the hybridization strength increases as n increases; ΔE with SOC decreases up to $n = 2$ and changes its sign. Conclusively, as n increases, the hybridization strength exceeds the SOC, resulting in the topological phase transition from TI to BI.

In Figs. 3(a) and 3(b), electronic band structures from the slab geometry of the $n = 1$ and 3 composition of $Pb_nBi_2Se_{n+3}$, which consist of six septuple and four hendecuple layers with 78.4 and 85.3 Å, respectively, are shown. Consistent with the critical SOC ratio in Fig. 2(a), $PbBi_2Se_4$ has a topologically protected surface state, whereas there is no such state connecting the valence and conduction bands in the $Pb_3Bi_2Se_6$ slab. This is further evidence of the change in Z_2 topological number from 1 to 0 as n increases. The 2D surface-state Dirac cone in the $PbBi_2Se_4$ slab is robust under the presence of nonmagnetic perturbations. Again, the 0.35-eV gap originating from bulk states is useful for high-temperature spintronics applications. In other words, a single isolated surface-state Dirac cone is seen in the energy range from -0.03 eV below the Fermi level to 0.32 eV above. Investigating the spin state of the surface state reveals that the directions of spin and momentum are locked and have a 90° angle between them, resulting in the circulation around the Dirac point as in other known TI materials such as Bi_2Se_3. Therefore, the surface state of $PbBi_2Se_4$ shows the spin-momentum locked 2D chiral Dirac fermion dispersion described as $v_F\vec{\sigma} \cdot (\hat{z} \times \vec{p})$.[27] In the case of the $Pb_3Bi_2Se_6$ slab, due to the weak van der Waals–type interlayer interactions, no distinct surface state appears from the bulk BI states.

Among the Pb-based chalcogenides series, $Pb_2Sb_2Te_5$, whose critical SOC ratio is 0.96, is located quite close to

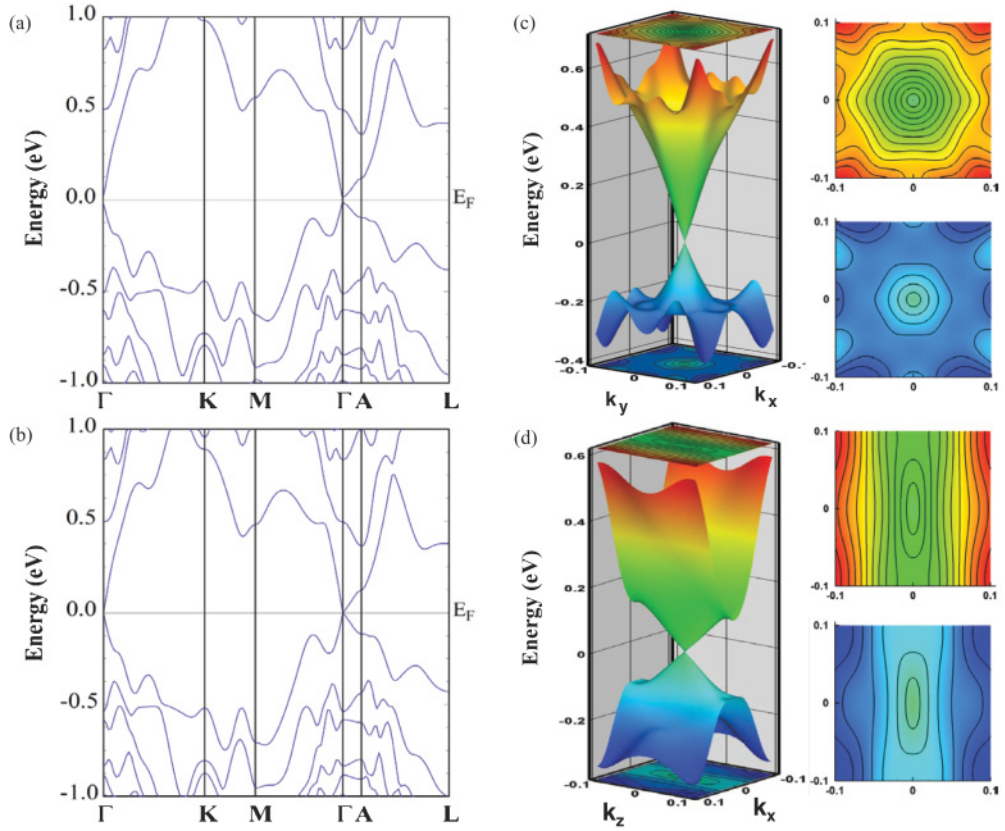

FIG. 4. (Color online) Band structures of $Pb_2Sb_2Te_5$ with (a) fully optimized crystal structure and (b) 0.5% reduction of ab-lattice constants. Three-dimensional plot of Dirac cone in (b) and its contours are shown in (c) and (d). Anisotropic Dirac cone dispersions on (c) k_x-k_y and (d) k_z-k_x plane.

the phase boundary, so that its Z_2 topological number may be easily tuned by changing external parameters. The 26-meV gap in the fully optimized geometry of $Pb_2Sb_2Te_5$ [Fig. 4(a)] is closed by making a small change in lattice constants. As shown in Fig. 4(b), $Pb_2Sb_2Te_5$, with a 0.5% reduction of the *ab*-lattice constants, is positioned exactly at the borderline of TI and BI, whose electronic band structure shows a gapless 3D Dirac cone at the Γ point, realizing monopoles that generate an inverse-square-type Berry curvature in the 3D Brillouin zone. A reduction of the *ab*-lattice constants makes the hybridization stronger, resulting in equilibration with the SOC strength. The band structure near the Dirac point shows anisotropic dispersions between in-plane and out-of-plane directions, described by a massless Dirac Hamiltonian

$$H = v_\perp \vec{\sigma}_\perp \cdot \vec{k}_\perp + v_\parallel \vec{\sigma}_\parallel \cdot \vec{k}_\parallel, \quad (1)$$

where $\vec{\sigma}$ are Pauli matrices, $\vec{k}_\perp$ is a momentum vector along the *c* axis, and $\vec{k}_\parallel$ is on the *ab* plane. A nearly circular cross section on the (k_x-k_y) plane and an ellipsoidal cross section on the (k_z-k_x) plane are depicted in Figs. 4(c) and 4(d), where the electronic band dispersion and the isoenergy contours of the 3D Dirac cone are shown.

The substitution of Te by Se might be useful to control the topological phase of this material in terms of varying both the SOC strength and lattice parameters. Considering the smaller ionic radius and SOC strength of Se than those of Te, the Se substitution can play a role in reducing not only lattice constants but also the SOC strength, both of which can accelerate the phase transition from TI to BI. Hence, $Pb_2Sb_2(Te_{1-x}Se_x)_5$ might be appropriate for studying the topological phase transition and the 3D Dirac cone.

In this work, we predicted new TI materials of Pb-based chalcogenides by investigating the change of the Z_2 topological number during variation of the SOC strength. With increasing *n* in the $Pb_nBi_2Se_{n+3}$ and $Pb_nSb_2Te_{n+3}$ series, the TI-to-BI transition occurs between $n = 2$ and 3. The series of TI materials covers a wide range of gap size from the largest to the smallest, which can be beneficial to practical applications. Among these compounds, $Pb_2Sb_2Te_5$ has a critical ratio of SOC strength close to 1, which indicates a closeness to the phase boundary. Both topological phases and the gap at the 3D Dirac cone are tunable by changing lattice constants or the SOC strength. Also, it will be interesting to investigate the physical properties of the bulk 3D Dirac cone manifested at the critical point. As an extension of the present work, the $Pb_n(Bi/Sb)_{2m}(Se/Te)_{n+3m}$ series, which are pseudobinary $[Pb(Se/Te)]_n[(Bi/Sb)_2(Se/Te)_3]_m$ systems and combinations of $Pb_n(Bi/Sb)_2(Se/Te)_{n+3}$ and $[(Bi/Sb)_2(Se/Te)_3]_m$ layered structures, are potential candidates for new TI materials that might show various bulk band gaps and topological phase transitions. The method used in our work may be the most appropriate tool to determine the Z_2 topological number of the systems without inversion symmetry, which show pair creation and annihilation of monopoles and antimonopoles at the topological phase-transition region.[16]

Support from the US DOE under Grant No. DE-FG02-88ER45372 (HJ, JHS, AJF) and the NSF under Grant No. DMR-0703882 (MGK) is gratefully acknowledged.

*jhsong@pluto.phys.northwestern.edu

[1] M. Z. Hasan and C. L. Kane, Rev. Mod. Phys. **82**, 3045 (2010).
[2] X.-L. Qi and S.-C. Zhang, Phys. Today **63**(1), 33 (2010).
[3] J. E. Moore, Nature (London) **464**, 194 (2010).
[4] C. L. Kane and E. J. Mele, Phys. Rev. Lett. **95**, 226801 (2005).
[5] C. L. Kane and E. J. Mele, Phys. Rev. Lett. **95**, 146802 (2005).
[6] F. D. M. Haldane, Phys. Rev. Lett. **61**, 2015 (1988).
[7] B. A. Bernevig, T. L. Hughes, and S.-C. Zhang, Science **314**, 1757 (2006).
[8] M. Konig, S. Wiedmann, C. Brune, A. Roth, H. Buhmann, L. W. Molenkamp, X.-L. Qi, and S.-C. Zhang, Science **318**, 766 (2007).
[9] L. Fu, C. L. Kane, and E. J. Mele, Phys. Rev. Lett. **98**, 106803 (2007).
[10] D. Hsieh, D. Qian, L. Wray, Y. Xia, Y. S. Hor, R. J. Cava, and M. Z. Hasan, Nature (London) **452**, 970 (2008).
[11] P. Roushan, J. Seo, C. V. Parker, Y. S. Hor, D. Hsieh, D. Qian, A. Richardella, M. Z. Hasan, R. J. Cava, and A. Yazdani, Nature (London) **460**, 1106 (2009).
[12] Y. Xia, D. Qian, D. Hsieh, L. Wray, A. Pal, H. Lin, A. Bansil, D. Grauer, Y. S. Hor, R. J. Cava, and M. Z. Hasan, Nat. Phys. **5**, 398 (2009).
[13] H. Zhang, C.-X. Liu, X.-L. Qi, X. Dai, Z. Fang, and S.-C. Zhang, Nat. Phys. **5**, 438 (2009).
[14] S. Chadov, X. Qi, J. Kubler, G. H. Fecher, C. Felser, and S. C. Zhang, Nat. Mater. **9**, 541 (2010).
[15] H. Lin, L. A. Wray, Y. Xia, S. Xu, S. Jia, R. J. Cava, A. Bansil, and M. Z. Hasan, Nat. Mater. **9**, 546 (2010).
[16] S. Murakami and S.-i. Kuga, Phys. Rev. B **78**, 165313 (2008).
[17] E. Wimmer, H. Krakauer, M. Weinert, and A. J. Freeman, Phys. Rev. B **24**, 864 (1981).
[18] J. P. Perdew, K. Burke, and M. Ernzerhof, Phys. Rev. Lett. **77**, 3865 (1996).
[19] A. H. MacDonald, W. E. Pickett, and D. D. Koelling, J. Phys. C **13**, 2675 (1980).
[20] The SOC strength depends on the radial integral part of the SOC matrix elements in the second variational approach. To control the SOC strength ratio, the radial integral part was multiplied by a simple constant.
[21] K. A. Agaev and S. A. Semiletov, Kristallografiya **13**(2), 258 (1968).
[22] L. E. Shelimova, O. G. Karpinskii, T. E. Svechnikova, E. S. Avilov, M. A. Kretova, and V. S. Zemskov, Inorg. Mater. **40**, 1264 (2004).
[23] K. A. Agaev, A. G. Talybov, and S. A. Semiletov, Kristallografiya **11**(5), 736 (1966).
[24] D. M. Bylander and L. Kleinman, Phys. Rev. B **41**, 7868 (1990).
[25] R. Asahi, W. Mannstadt, and A. J. Freeman, Phys. Rev. B **59**, 7486 (1999).
[26] The selected points where the band inversion occurs with increasing SOC are the *Z* point for $n = 1,3$ and the Γ point for $n = 2$, in both series of Pb chalcogenides.
[27] D. Hsieh, Y. Xia, D. Qian, L. Wray, J. H. Dil, F. Meier, J. Osterwalder, L. Patthey, J. G. Checkelsky, N. P. Ong, A. V. Fedorov, H. Lin, A. Bansil, D. Grauer, Y. S. Hor, R. J. Cava, and M. Z. Hasan, Nature (London) **460**, 1101 (2009).